

Turning noise into signal: learning from the scatter in the Hubble diagram

Tiago Castro, Miguel Quartin, Sandra Benitez-Herrera

Instituto de Física – Universidade Federal do Rio de Janeiro, 21941-972, Rio de Janeiro, RJ, Brazil

Abstract

The supernova (SN) Hubble diagram residual contains valuable information on both the present matter power spectrum and its growth history. In this paper we show that this information can be retrieved with precision by combining both peculiar velocity and weak-lensing analysis on the data. To wit, peculiar velocity induces correlations on the nearby SN while lensing induces a non-Gaussian dispersion in faraway objects. We show that both effects have almost orthogonal degeneracies and discuss how they can be extracted simultaneously from the data. We analyze the JLA supernova catalog in a 14-dimensional parameter space, assuming a flexible growth-rate index γ . We arrive at the following marginalized constraints: $\sigma_8 = 0.65^{+0.23}_{-0.37}$ and $\gamma = 1.38^{+1.7}_{-0.65}$. Assuming instead GR as the correct gravitation theory (and thus $\gamma \equiv 0.55$), the constraints in σ_8 tighten further: $\sigma_8 = 0.40^{+0.21}_{-0.23}$. We show that these constraints complement well the ones obtained from other datasets and that they could improve substantially with more SNe.

Keywords: peculiar velocity – gravitational lensing: weak – cosmology: observations – cosmological parameters – large-scale structure of the universe – stars: supernovae: general

1. Introduction

Type Ia supernovae (SNe) are still the only established high-redshift standard candles, with an intrinsic dispersion σ_{int} of less than 0.15 in magnitude after standardization (Hamuy et al., 1996; Riess et al., 1996). In the late 90s, using a sample of about 50 of these objects the discovery of the accelerated expansion was established by Riess et al. (1998); Perlmutter et al. (1999). The confidence in that result was enhanced soon after in Bahcall et al. (1999) by combining the SNe with galaxy surveys early Cosmic Microwave Background (CMB) data on large-scales. It is nowadays a well-established result, with strong evidence coming from observations of the Baryonic Acoustic Oscillations (Eisenstein et al., 2005; Blake et al., 2011) and of the anisotropies of the CMB (Ade et al., 2015).

Since those pioneering works, a vast number of SNe surveys have been conducted, and more are underway or planned. This will increase the number of observed explosions from the current $\sim 10^3$ (Betoule et al., 2014) to over 10^6 (Abell et al., 2009). However, although the statistical uncertainty associated with the intrinsic dispersion in magnitude will consequently be improved by more than one

order of magnitude, it will be a daunting task to improve the systematics at the same rate. These are therefore likely to become dominant in the upcoming large datasets.

Interestingly, this increasing contamination from systematics opens up new opportunities. In particular, a good part of this extra “noise” in the Hubble diagram can be converted into “signal” by modeling two independent astrophysical effects: peculiar velocities (PV) and gravitational lensing. The former introduces correlations in the supernova magnitudes for $z \lesssim 0.1$ (Gordon et al., 2007). The latter introduces a redshift-dependent non-Gaussian scatter in the distribution of the supernovae and was first discussed in Bernardeau et al. (1997); Hamana and Futamase (2000); Valageas (2000). Contrary to peculiar velocities, lensing introduces *no* correlations among the supernovae,¹ and is moreover only relevant for high redshift events ($z \gtrsim 0.4$). These new sources of signal allow the SNe to transcend their background role and constrain cosmological perturbation parameters.

¹Unless more than one SNe have really small angular separation and happen to be lensed by the same structure.

In the case of lensing, this idea was proposed a decade ago by [Dodelson and Vallinotto \(2006\)](#), and recently developed further in [Quartin et al. \(2014\)](#); [Castro and Quartin \(2014\)](#) in what was called the Method of the Moments (MeMo). The idea behind it is rather simple. The apparent magnitude of standard candles depends on the gravitational perturbations crossed by their light along its geodesic. The geodesic is deflected by any intervening matter, but the effect is in practice dominated by the distribution of matter on the largest scales. Thus, if we analyze the statistical distribution of the SNe apparent magnitudes around their mean value, we can constrain properties of the intervening matter, like the amplitude of the linear perturbations or parameters of the halo model.

The weak-lensing effect can be encapsulated in the convergence lensing PDF, which gives the probability density of having a given convergence (and thus a given magnification, as to first order the shear can be neglected) as a function of redshift. This PDF was shown to have an approximate log-normal shape in [Holz and Linder \(2005\)](#); [Marra et al. \(2013\)](#) (see [Appendix C](#) for one caveat though), the large skewness of which related to the fact that relatively few objects are behind clusters and thus get magnified: the large majority of geodesics come instead through cosmic voids, and thus get demagnified – although see [Bolejko et al. \(2013\)](#). It can be computed using ray-tracing techniques on N-body simulations. However, this method is computationally too expensive to carry out likelihood analysis, so [Kainulainen and Marra \(2009, 2011\)](#) developed a fast stochastic method called sGL to compute the lensing PDF. The sGL relies on prescriptions for the mass function ([Jenkins et al., 2001](#); [Sheth and Tormen, 1999](#); [Courtin et al., 2011](#)) and for the concentration parameter ([Zhao et al., 2009](#)) as a function of cosmology. It yields results which are consistent both with the dark matter N-body simulations of [Hilbert et al. \(2008\)](#); [Takahashi et al. \(2011\)](#), with the theoretical calculations of [Ben-Dayan et al. \(2013\)](#) and with the experimental data of [Jönsson et al. \(2010a,b\)](#).

The lensing gets convolved with the intrinsic SNe distribution ([Amendola et al., 2010](#); [Quartin et al., 2014](#)), which dilutes the non-Gaussianity. The MeMo consists in parametrizing the lensing PDF by the first moments of the distribution, which can then be propagated into the moments of the final convolved PDF and confronted with data. [Quartin et al. \(2014\)](#) showed that this could be used

to constrain σ_8 to the percent level with 10^6 SNe. In [Amendola et al. \(2015\)](#) it was shown that SNe lensing can also be used to constrain modified gravity models through its effect on the growth-rate.

In practice, in order to model the lensing-induced scatter some assumptions on the intrinsic scatter of SNe are required; in particular, we assume that it is not strongly dependent on redshift. In fact, a constant scatter was shown to be currently a reasonable hypothesis using Bayesian analysis ([Castro and Quartin, 2014](#)) and it also agrees with the underlying motivation for using SNe as standard candles whose properties do not depend on distance.

The effect of peculiar velocities on the supernova is altogether different, and was developed in detail by [Hui and Greene \(2006\)](#); [Davis et al. \(2011\)](#). It starts from the fact that the Hubble diagram should in principle be built using the cosmological redshift, that is, the one due to the expansion of the universe. In practice this is not an easy task as the measured redshifts are affected by non-cosmological effects arising from the gravitational potential at the source and around us, and by the peculiar motions of the standard candles and of the observer. The combination of cosmological z_{cosmo} , peculiar velocity z_{pec} and gravitational z_{grav} redshifts gives the observed redshift z_{obs} :

$$(1 + z_{\text{obs}}) = (1 + z_{\text{cosmo}})(1 + z_{\text{pec}})(1 + z_{\text{grav}}). \quad (1)$$

The last two terms are systematic effects that need to be accounted for. In terms of magnitudes, a bias δz corresponds to a bias $\delta m = \delta z \, dm/dz$. The nature of the Hubble diagram makes these corrections in magnitude large for low redshifts, where the slope is very steep.

The correction for our own velocity is straightforward: assuming our velocity to be the only contribution to the CMB dipole, Planck infers the following (curiously mnemonic) value: $\beta_0 = (1.2345 \pm 0.0007) \times 10^{-3}$ [Adam et al. \(2015\)](#). This assumption is theoretically well motivated (we only expect the non-kinetic dipole to be $\mathcal{O}(10^{-5})$ like the other multipoles), and in any case it is not an untested one: our velocity also induces an aberration in the sky. This was shown to be detectable by Planck in [Kosowsky and Kahnishvili \(2011\)](#); [Amendola et al. \(2011\)](#), and consequently measured in the data by [Aghanim et al. \(2014\)](#), although with only 36% precision (considering systematics). [Notari and Quartin \(2012\)](#) showed that this error bar could be reduced to less than 10% in future CMB experiments. [Yoon and Huterer \(2015\)](#) also derived that

a 20% precision might be possible by measuring the kinematic dipole with future galaxy surveys.

The peculiar velocities of the SNe themselves are harder to account for. They are often just modeled as Gaussian random terms, which are included in the covariance matrix calculation. A random velocity $v = 300$ km/s corresponds to an uncertainty $\sigma_m^{\text{pec}} = 0.2$ mag for objects at redshift $z = 0.01$, but only $\sigma_m^{\text{pec}} = 0.02$ mag at $z = 0.1$ (Davis et al., 2011). The SNe velocities are however not really random, as the large-scale gravitational potential wells incur in coherent velocity flows, which extend to many dozens of Mpc (Hoffman et al., 2015). As discussed in Hui and Greene (2006), any two SNe in the same region of the sky will have therefore correlated magnitude fluctuations. In a nutshell, if a given supernovae is dimmer than the average because it is moving away from us, a nearby supernova has an *excess probability* of also being dimmer than average because it will be in the same velocity flow. Moreover, very low- z galaxies should have peculiar velocities correlated to our own Milky Way's. These corrections should in principle not be ignored, lest we introduce biases to the inferred cosmological parameters (Neill et al., 2007; Gordon et al., 2007). Some supernovae catalogs try to avoid this issue simply by not including supernovae below redshift ~ 0.01 . As we discuss below, we can (and should) easily subtract from the data the effects from our peculiar velocity using the measurements of the CMB dipole. This should remove this possible bias, even for SNe with redshift below 0.01.

Importantly, the amplitude of the above correlations depend on cosmology, and it was realized in Bonvin et al. (2006) that this would open a new avenue of research. As these correlations are directly related to the 2-point correlation function of matter and, therefore, to the matter power spectrum, it was soon realized in Gordon et al. (2007) that even a 271 supernovae catalog available at the time was able to put the impressive constraint $\sigma_8 = 0.79 \pm 0.22$. A similar idea was proposed also in Hannestad et al. (2008). Abate and Lahav (2008) further developed the idea to show that it could be used to measure also the growth of perturbations.

Both lensing and PV are thus new sources of signal, and each allows the SNe to transcend their background role and constrain cosmological perturbation parameters. In this paper we develop a simple technique to combine them together and show that these two probes are very complementary. We develop the technique of using PV in detail and

adapt the Joint Lightcurve Analysis (JLA) supernova catalog (Betoule et al., 2014) in order to do so. We show that combining together PV and lensing allows one to break the degeneracy between σ_8 (which is directly related to the the amplitude of the power spectrum, as per Eq. (16) below) and the index of growth-rate of matter perturbations γ .

This paper is organized as follows: in Section 2 we review the peculiar velocity effects in the Hubble diagram; in Section 4 we review the JLA catalog and adapt it for measuring the PV; in Section 3 we develop a simple technique to combine PV and lensing effects in supernova analysis; in Section 5 we show the derived constraints on the power spectrum parameters and compare the results with the ones obtained from other datasets; finally, we discuss the conclusions and perspectives in Section 6. We also provide some technical details on our Monte Carlo Markov chain analysis in Appendix A, on our search for systematics in the data in Appendix B and on our mock catalog tests in Appendix C.

2. The effect of peculiar velocities on the Hubble diagram

2.1. The effect on distances and magnitudes

In terms of the peculiar velocities, Eq. (1) can be approximated as (Hui and Greene, 2006; Davis et al., 2011)

$$(1 + z_{\text{obs}}) = (1 + z_{\text{cosmo}})(1 + \beta_{\text{SN}} \cdot \hat{\mathbf{n}} - \beta_{\text{o}} \cdot \hat{\mathbf{n}}), \quad (2)$$

where β_{SN} and β_{o} are the peculiar velocities (in units of the speed of light) of the supernovae and of our own peculiar motion, respectively; $\hat{\mathbf{n}}$ is the unit vector for the direction between the observer and SNe. Peculiar velocities affect not only z_{obs} , but as shown by Hui and Greene (2006) also directly the luminosity of the sources due to the aberration effect, which changes the angular size of the objects much like gravitational lensing. The observed luminosity distance d_L is thus related to the cosmological distance \bar{d}_L by:

$$d_L(z_{\text{obs}}) = \bar{d}_L(z_{\text{cosmo}})(1 + 2\beta_{\text{SN}} \cdot \hat{\mathbf{n}} - \beta_{\text{o}} \cdot \hat{\mathbf{n}}), \quad (3)$$

with \bar{d}_L given by:

$$\bar{d}_L(z) = (1 + z) \int_0^z \frac{c}{H(z')} dz'. \quad (4)$$

The quantity of interest is the change $\delta_{d_L}(z)$ in d_L at the observed redshift:

$$\delta_{d_L}(z_{\text{obs}}) = \frac{[d_L(z_{\text{obs}}) - \bar{d}_L(z_{\text{obs}})]}{\bar{d}_L(z_{\text{obs}})}. \quad (5)$$

If we Taylor expand \bar{d}_L , we can rewrite the above equation as

$$\delta_{d_L}(z_{\text{obs}}) = \beta_{\text{SN}} \cdot \hat{\mathbf{n}} - \frac{(1+z_{\text{obs}})^2(\beta_{\text{SN}} - \beta_{\text{o}})}{H(z_{\text{obs}})d_L(z_{\text{obs}})} \cdot \hat{\mathbf{n}}. \quad (6)$$

Using the relation between magnitudes and luminosity distances

$$m = 5 \log_{10} \left(\frac{d_L}{10 \text{Mpc}} \right) + M, \quad (7)$$

and the equations for d_L and \bar{d}_L we can both correct the JLA magnitudes and remove the dipole term (β_{o}) from \bar{d}_L . The corresponding change in magnitude is

$$\delta_m = \left(1 + \frac{1+z_{\text{obs}}}{H\chi} \right) (\beta_{\text{SN}} \cdot \hat{\mathbf{n}} - \beta_{\text{o}} \cdot \hat{\mathbf{n}}). \quad (8)$$

Finally, aberration also causes the change in apparent position of the sources in the sky, and thus the inferred distance between them. This effect is not usually discussed in the literature, and to our knowledge has been so far ignored, possibly on the grounds that in practice the overall effect is small. We nevertheless discuss this in Section 4.

2.2. Peculiar Velocity covariance

From now on we will denote the observed redshift z_{obs} as just z for simplicity of notation.

The velocity correlation function is defined by

$$\xi(\mathbf{r}_i, \mathbf{r}_j) \equiv \langle (\beta_{\text{SN}}(\mathbf{r}_i) \cdot \hat{\mathbf{r}}_i)(\beta_{\text{SN}}(\mathbf{r}_j) \cdot \hat{\mathbf{r}}_j) \rangle, \quad (9)$$

where $\hat{\mathbf{r}}_i, \hat{\mathbf{r}}_j$ are the unit vectors pointing toward SNe i and j , respectively, and $\beta_{\text{SN}}(\mathbf{r}_i), \beta_{\text{SN}}(\mathbf{r}_j)$ are the corresponding SN velocity vectors. Since the velocity correlation function must be rotationally invariant, it can be decomposed in two components in terms of the comoving separation r between SNe

$$\xi(\mathbf{r}_i, \mathbf{r}_j) = \sin \theta_i \sin \theta_j \xi_{\perp}(r, z_i, z_j) + \cos \theta_i \cos \theta_j \xi_{\parallel}(r, z_i, z_j), \quad (10)$$

with $\mathbf{r}_{ij} \equiv \mathbf{r}_i - \mathbf{r}_j$; $r = |\mathbf{r}_{ij}|$; $\cos \theta_i \equiv \hat{\mathbf{r}}_i \cdot \mathbf{r}_{ij}$ and $\cos \theta_j \equiv \hat{\mathbf{r}}_j \cdot \mathbf{r}_{ij}$. The parallel and perpendicular components of the velocity function are given by

$$\xi_{\parallel, \perp} = G'(z_i)G'(z_j) \int_0^\infty \frac{dk}{2\pi^2} P(k) K_{\parallel, \perp}(kr), \quad (11)$$

where G is the growth function, $K_{\parallel} \equiv j_0(x) - 2j_1(x)/x$, $K_{\perp}(x) \equiv j_1(x)/x$ and j_0, j_1 represent the

spherical Bessel functions. For the diagonal $i = j$ terms, we have simply:

$$\xi(\mathbf{r}_i, \mathbf{r}_i) = [G'(z_i)]^2 \int_0^\infty \frac{dk}{2\pi^2} \frac{P(k)}{3}. \quad (12)$$

The peculiar-motion covariance matrix is finally given by

$$C_v(i, j) = \left[1 - \frac{(1+z_i)^2}{H(z_i)d_L(z_i)} \right] \left[(\dots)_{i \rightarrow j} \right] \xi(\mathbf{r}_i, \mathbf{r}_j). \quad (13)$$

Here, we extend the above usual analysis to include non-standard growth rates. This allows one to account for scenarios that go beyond the standard Λ CDM model. We employ the common parametrization for the linear growth rate f (Lahav et al., 1991)

$$f(z) = -\frac{d \ln G}{d \ln(1+z)} \simeq \Omega_m(z)^\gamma, \quad (14)$$

where γ is the growth rate index and $\Omega_m(z) = \Omega_{m0}(1+z)^3 H_0^2/H^2(z)$. Within General Relativity (GR) and for the standard Λ CDM model f is accurately described by Eq. (14) with $\gamma = \gamma_{\Lambda\text{CDM}} \approx 0.55$. It can be shown that the γ parameter does not depend strongly on w_{DE} , the equation of state parameter of dark energy (Amendola and Tsujikawa, 2010) – see also Fig. 7b of Mantz et al. (2015). Therefore, γ is often employed as a simple way of describing the growth-rate in modified gravity models.

Figure 1 illustrates the physical effect of the PV's in the Hubble diagram. Because of the PV, the Hubble residual (the difference between the SNe magnitudes and the best-fit cosmology) becomes correlated. In this figure, in order to make the effect clear by eye, we assume an idealized case where the SNe have no intrinsic dispersion, i.e. $\sigma_{\text{int}} = 0$, and are scattered in a small area — if the same SNe are distributed over a larger (smaller) area, the effect is diminished (enhanced). In particular, we show three random realizations generated using 500 supernovae equally scattered both in redshift and in an area of the sky of 400 deg^2 . These are possible samples of these 500 SNe: we drew 3 samples of a 500 dimensional multi-normal distribution, with zero mean and a covariance matrix given by Eq. (13) for a fiducial cosmological model with parameters close to the best-fit from Planck Ade et al. (2015). To compute Eq. (13) we employed the code made available in Hui and Greene (2006).²

²<http://www.astro.columbia.edu/~lhui/PairV/>

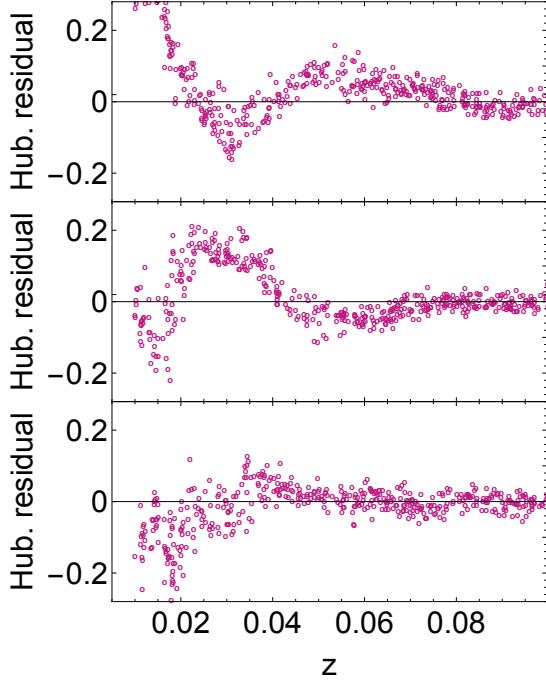


Figure 1: Illustration of the physical effect of velocities in the Hubble diagram residual for three random realizations. In all cases we assumed 500 idealized SNe (without intrinsic dispersion – $\sigma_{\text{int}} = 0$) in the range $0 < z < 0.1$ over a square 400 deg^2 area. In these idealized cases the correlations are easily noticed by eye. In practice, these are suppressed by much larger intrinsic dispersion of the SNe.

2.3. Likelihood parameters

For the likelihood analysis, we used

$$L_{\text{PV}} \propto \frac{1}{\sqrt{|\Sigma_{\text{PV}}|}} \exp \left[-\frac{1}{2} \delta_m^T \Sigma_{\text{PV}} \delta_m \right], \quad (15)$$

where $\Sigma_{\text{PV}} = C_{\text{JLA}}(i, j) + C_v(i, j)$ is the full PV covariance matrix. The term $C_{\text{JLA}}(i, j)$ is the covariance presented in Eq. (13) of [Betoule et al. \(2014\)](#) (that combines terms from intrinsic dispersion of SN magnitudes, the uncertainty in the measurements from: statistics, calibration, model, bias, host, contamination, and dust; and degradation due to both lensing and peculiar velocities), minus two contributions: the peculiar velocity and intrinsic dispersion terms. The original JLA peculiar velocity covariance has two terms: one linear and one non-linear. The non-linear part is encapsulated in a simple parametrization: the diagonal matrix given by $(5\sigma_v)/(z \log 10)$. The linear part is given by the matrix in (13). The intrinsic dispersion term originally had different values depending in which

survey observed the supernova. Here, we replace it assuming a single value σ_{int} invoking Occam’s Razor because we do not think these extra parameters are needed. Furthermore, as can be seen in Fig. (7) of [Betoule et al. \(2014\)](#), a constant dispersion is a good fit in the range of our PV analysis.

The matter power spectrum was evaluated numerically using CAMB ([Lewis et al., 2000](#)) in a 14-dimensional parameter space sampled by a Markov Chain Monte Carlo (MCMC) method. For cosmology we assume a model with the same background expansion as a flat Λ CDM and composed of 6 parameters: $\{\Omega_{c0}, \Omega_{b0}, \gamma, h, n_s, A \exp(-2\tau)\}$, where h is H_0 in units of $100 \text{ km}/(\text{s.Mpc})$. These 6 are complemented by a set of 8 nuisance parameters: one is the SNe intrinsic magnitude M , three $(\alpha, \beta, \delta M)$ are from the standard SALT2 analysis, one (σ_v) stands for a random component attributed to the non-linear velocity dispersions, two $(\sigma_{\text{int}}^{\text{low } z}, \sigma_{\text{int}}^{\text{hi } z})$ for the intrinsic dispersion of the SNe, and one $(\mu_{3, \text{int}})$ for the intrinsic skewness of the SNe. These last three are important for the lensing analysis. From these 14 parameters we derive another two: $\Omega_{m0} \equiv \Omega_{c0} + \Omega_{b0}$ and, from the resulting matter power spectrum $P(k)$, the standard deviation of density perturbations on $8 \text{ Mpc}/h$ spheres:

$$\sigma_8 \equiv \sqrt{\int dk \frac{k^2}{2\pi^2} \frac{9 P(k)}{(kR)^6} [\sin(kR) - kR \cos(kR)]^2}, \quad (16)$$

where $R \equiv 8 \text{ Mpc}/h$.

It was shown in [Marra et al. \(2013\)](#) that the lensing of SNe is not very sensitive to the value of a constant w_{DE} . Likewise, as discussed above in Section 2.2 the growth rate index γ is also not very sensitive to w_{DE} . We thus assume for simplicity $w_{\text{DE}} \equiv w_{\Lambda} \equiv 1$ in our analysis.

Since SNe PV alone is not currently able to measure h , n_s or Ω_{b0} with any significant sensitivity, we adopted the prior $h = 0.696 \pm 0.007$ from [Bennett et al. \(2014\)](#) and $\Omega_b h^2 = (0.021 \pm 0.01)$ from Big Bang Nucleosynthesis (BBN) [Iocco et al. \(2009\)](#). For n_s we allowed a broad tophat in the range $[0.9 - 1.0]$. All other priors were assumed flat and much wider than the likelihood. See [Appendix A](#) for more details on our MCMC implementation.

3. Combined analysis of PV and lensing

Lensing on supernovae data was another effect that until recent works was merely treated as a nuisance systematic on supernovae magnitudes. The

Method of the Moments (MeMo) was first presented in [Quartin et al. \(2014\)](#) and further enhanced in [Castro and Quartin \(2014\)](#), where it was also tested with real data. It extends the traditional analysis to the higher moments of the Hubble diagram residual, and allows one to probe the matter properties intervening supernovae and observer. The MeMo analysis is basically a χ^2 approach capable of quantifying the likelihood that a given sample was generated by a given observed PDF.

The important quantities of the MeMo are the sample moments of the distribution. It was shown by [Quartin et al. \(2014\)](#) that, concerning supernovae lensing, basically all the signal is contained in the first 4 moments (and most of it in the first 3). So, the MeMo likelihood of a supernovae sample distributed in a redshift bin z_k is well approximated by:

$$L_{\text{MeMo}}(z_k) = \frac{1}{(2\pi)^2 \sqrt{|\Sigma_{\text{MeMo}}|}} \exp\left(-\frac{1}{2} \chi_k^2\right),$$

$$\chi_k^2 = (\boldsymbol{\mu} - \boldsymbol{\mu}_{\text{data}})^t \Sigma_{\text{MeMo}}^{-1} (\boldsymbol{\mu} - \boldsymbol{\mu}_{\text{data}}),$$

$$\boldsymbol{\mu} \equiv \{\mu'_1, \mu_2, \mu_3, \mu_4\}, \quad (17)$$

where the $\{\boldsymbol{\mu}, \boldsymbol{\mu}_{\text{data}}\}$ are the first moment and the second to fourth central moments of the observed PDF and the given sample respectively. The formula of the full covariance matrix Σ_{MeMo} involves all moments up to the 8th, and the full equation was obtained in [Quartin et al. \(2014\)](#). In order to compute it, we employ the `turboGL`³ code, which implements the sGL method discussed in Section 1.

The observed supernovae PDF is a result of the convolution of the lensing PDF with the supernovae intrinsic distribution. The lensing PDF was obtained using the sGL method discussed in Section 1. Following [Castro and Quartin \(2014\)](#), the supernovae intrinsic distribution was parametrized by two nuisance parameters: its intrinsic variance and skewness (respectively σ_{int}^2 and $\mu_{3,\text{int}}$). The degenerescence between the intrinsic moments and the lensing ones is broken due to the hypothesis that the intrinsic moments do not evolve with redshift. This hypothesis was strongly preferred by data in a Bayesian model selection and also agrees with the idea that the properties of a standard candle do not evolve with redshift. Therefore the observed

SNe PDF moments are given by:

$$\begin{aligned} \mu_2 &= \mu_{2,\text{lens}} + \sigma_{\text{int}}^2, \\ \mu_3 &= \mu_{3,\text{lens}} + \mu_{3,\text{int}}, \\ \mu_4 &= \mu_{4,\text{lens}} + 6 \mu_{2,\text{lens}} \sigma_{\text{int}}^2 + 3 \sigma_{\text{int}}^4. \end{aligned} \quad (18)$$

Regarding the sample moments, we suggested in [Castro and Quartin \(2014\)](#) that the best variable to compute the central moments is through the random variable:

$$m_{j,k} = m_{j,k}^{\text{catalog}} - m_{\text{best}}(z_k) + m_{\text{best}}(z_j), \quad (19)$$

where j and k are the j -th supernova in the k -th bin. This is exactly as calculating the moments directly on the minimized Hubble residual diagram. Here we take a more robust approach and adapt this variable in order to include also the SALT-2 nuisance parameters. The supernovae magnitudes inferred through the SALT-2 light curve fitting are given by the following relation:

$$m_{\text{catalog}} = m_B^* - M - \Delta M + \alpha x - \beta c, \quad (20)$$

where m_B^* , x and c are results from SALT-2 light curve fitting and M , ΔM , α and β are calculated minimizing the Hubble residual. Here, instead of using the moments calculated in the minimized Hubble residual, we calculate them as a function of the cosmological background parameters and the four SALT-2 nuisance parameters. Hence, our results of the MeMo analysis in this paper are slightly different from our previous work due to the marginalization over these nuisance parameters.

Note that although in principle Σ_{MeMo} depends on cosmology, [Quartin et al. \(2014\)](#) showed that to good approximation one can fix the cosmology just keeping the redshift dependence. In that paper we did not have any light-curve fitting nuisance parameters, so here we compute it including them. So we have $\Sigma_{\text{MeMo}}(z, \alpha, \beta, M, \Delta M)$.

The complementarity of the peculiar velocity (only sensitive to low- z supernovae) and lensing (sensitive to medium to high- z supernovae) signals motivates the analysis of these effects in an independent way. We therefore just need to compute two likelihoods, one for SNe in $z < 0.1$ including the PV covariance, and one for SNe with $z \geq 0.1$ including the higher moments, and multiply both to get the total constraints:

$$L_{\text{tot}} = L_{\text{PV}} L_{\text{MeMo}}. \quad (21)$$

³turbogl.org

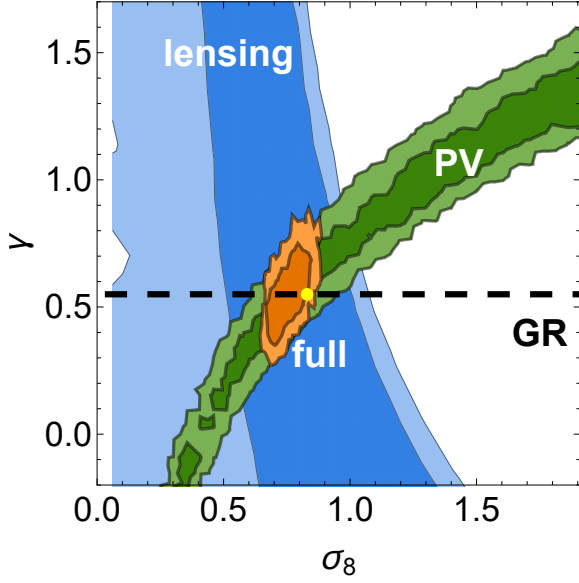


Figure 2: 1 and 2σ forecast for a possible future SNe catalog consisting of 3000 DES plus 1000 low-redshift SNe uniformly distributed in the range $0.01 < z < 0.1$ and in an area of the sky of 400 deg^2 . We show the contours obtained by using only the peculiar velocities (PV) method (green), using only the MeMo method (blue), or both combined (orange). The dashed black line represents the expectation from GR. Lensing and PV show good complementarity: the degeneracy lines make a $\sim 60^\circ$ angle around the fiducial point.

To illustrate the potential of such a combined analysis, we made a forecast for a possible future SNe catalog consisting of 3000 Dark Energy Survey (DES) supernovae, with the redshift distribution and error estimates made in [Bernstein et al. \(2012\)](#) (we adopt their “hybrid5” catalog), plus 1000 low-redshift SNe uniformly distributed in the range $0.01 < z < 0.1$ and in an area of the sky of 400 deg^2 , with an intrinsic scatter of 0.13 mag . This is a very simplistic low- z catalog. In reality, for a given telescope the distribution will be a combination of many factors: the fact that the observed volume grows as z^2 , the cadence of observations, the integration time, etc. More realistic estimates will inevitably feature proportionally less events at very low z . But since the idea here with this forecast is more to illustrate the method, we leave a more detailed forecast for future investigations.

Figure 2 depicts the contours obtained with L_{PV} , L_{MeMo} and L_{tot} separately. The combined contours provide a precise measurement of both σ_8 and γ : the uncertainties are $\simeq 0.1$ and $\simeq 0.2$, respectively. Clearly, in this case most constraining power is coming from PV, so we plan to conduct in a future pa-

per a careful analysis of the optimal observational strategy to detect SNe for measuring their PV correlations. As can be seen from the plot, the contours show good complementarity, and the degeneracy directions around the best fit subtend an angle of $\sim 60^\circ$. This nicely illustrates the benefit of combining different probes: the constraints coming solely from either PV or lensing exhibit pronounced parameter degeneration.

4. Adjusting the JLA catalog for PV measurements

In this paper we make use of the Joint-Lightcurve Analysis (JLA) sample ([Betoule et al., 2014](#)) consisting of 740 objects. All SNe were spectroscopically confirmed and with high quality light-curve data, and light-curve calibration was performed using the SALT2 model of [Guy et al. \(2007\)](#) with significant improvements with respect to the previous analysis of [Conley et al. \(2011\)](#). The dataset is well sampled in redshift up to $z \simeq 1$. The angular distribution of the SNe, on the other hand, is far from homogeneous. It is basically constituted of 4 deep fields, the mid-depth stripe-82 and a reasonably homogeneous low- z sample. The spatial distribution of these 740 SNe are depicted in Figure 3. All our lensing signal therefore comes from these few deep fields, and most of our PV signal comes from the Stripe-82 due to the angular proximity of the SNe.

In the original JLA analysis the peculiar velocity model for the low- z sample was left unchanged with respect to the analysis of [Conley et al. \(2011\)](#), where they correct for peculiar motion on a SN-by-SN basis. This approach follows the prescription of [Hui and Greene \(2006\)](#) and consists on a two-step correction, first applied to redshifts through a slightly different version of Eq. (2):

$$(1 + z_{\text{obs}}) = (1 + z_{\text{cosmo}})(1 + \beta_{\text{SN}} \cdot \hat{n} - \beta_o \cdot \hat{n}), \quad (22)$$

where z_{obs} is the observed redshift and z_{cosmo} is the redshift with respect to the CMB rest-frame.⁴ The second step consists of a (much smaller) correction to the observed magnitude by adding the term $-5 \log_{10}(1 + \beta_{\text{SN}} \cdot \hat{n})$.

Therefore in order to use the JLA catalog for peculiar velocities measurements it is better to undo the second step of this analysis to obtain the raw

⁴We name it so because, aside any gravitational redshifts, it coincides with the pure cosmological expansion redshift.

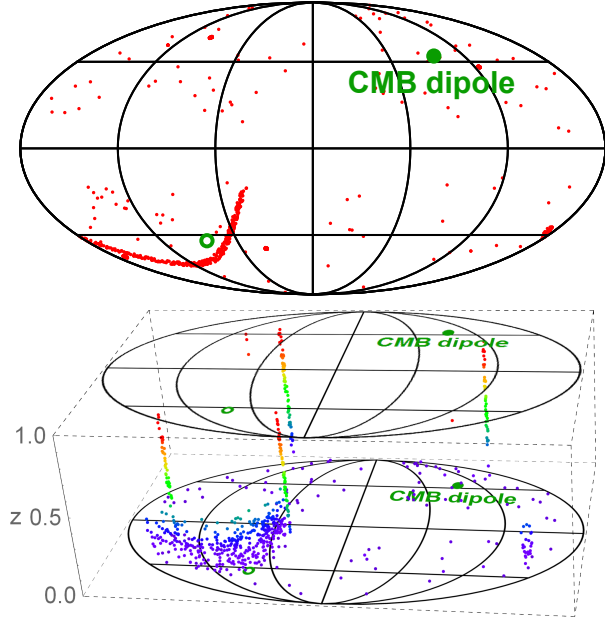


Figure 3: *Top*: The spatial distribution of the JLA catalog in galactic coordinates, in the Mollweide projection. We also depict the CMB dipole direction with a full green circle and its antipode with an open circle. *Bottom*: Similar plot but with a third dimension added to show also the redshift (with dots colored from purple to green to red as z increases). Note that the catalog is mostly constituted of 4 deep fields, the mid-depth stripe-82 and low- z SNe scattered around the sky.

magnitudes (magnitudes that have the expected correlations between the supernovae). To undo this correction one needs $\beta_{\text{SN}} \cdot \hat{n}$, the component of the peculiar velocity of the supernovae in the line of sight of the observer. This can be done by direct inversion of Eq. (22). JLA provides both z_{cosmo} and z_{obs} , and $\beta_{\text{o}} \cdot \hat{n}$ is also known (assuming the kinematic explanation to the CMB dipole). We thus have:

$$1 + \beta_{\text{SN}} \cdot \hat{n} = \frac{1 + z_{\text{obs}}}{1 + z_{\text{cosmo}}} + \beta_{\text{o}} \cdot \hat{n}. \quad (23)$$

A minor point has to be emphasized about how JLA catalog computes the z_{cosmo} . To obtain this they correct the catalog accordingly to an peculiar velocity model, first presented in [Hudson et al. \(2004\)](#), and combine it with LSS data. For more details see [Betoule et al. \(2014\)](#) and references therein. Although this estimation uses other data and is based on a model, we believe it is warranted since it does not assume a cosmological model and shares the same basic assumptions as our analysis (basically the Λ CDM model). In any case, as will be

pointed out in the end of this section, the correction on the magnitudes is sub-dominant.⁵

The raw magnitudes also have a dipole shift due to our own velocity in relation to the CMB rest frame. We have also removed this dipole using Eq. (4). Summarizing the magnitudes used in this analysis are given in relation of JLA magnitudes by:

$$m = m_{\text{JLA}} + 5 \log_{10}(1 + \beta_{\text{SN}} \cdot \hat{n}) - 5 \log_{10}(1 - \beta_{\text{o}} \cdot \hat{n}). \quad (24)$$

This correction, although sub-dominant, is warranted as we understand that the peculiar velocity analysis has to be done in the observed magnitudes corrected only by our peculiar velocity. That being said, the crucial correction is on the redshifts of the supernovae, which are changed due our velocity in relation of CMB rest frame, β_{o} – see Eq. (2).

Finally, as discussed in Section 2 one in principle should correct also the angular positions of the SNe due to the aberration effect. This affects the inferred separation of the SNe, but the overall effect is very small because if nearby objects share the same velocity flow, they will be equally aberrated and the effect on the correlation function will be zero. Moreover, most current SNe relevant for the PV signal happen to lie very close to the (antipode of) the CMB dipole direction (see Figure 3), where the aberration effect is at its minimum – see Eq. (4) of [Amendola et al. \(2011\)](#).

In any case, it is straightforward to remove the aberration induced by our own motion in the SNe catalog (the aberration induced by the SNe peculiar motion is trickier, because it requires an independent estimate of their velocity). Following [Challinor and van Leeuwen \(2002\)](#), the relation between the real position \hat{n}' of a given SNe and its observed position \hat{n} is:

$$\hat{n}' = \frac{\hat{n} \cdot \hat{\beta}_{\text{o}} - \beta_{\text{o}}}{1 - \hat{n} \cdot \beta_{\text{o}}} \hat{\beta}_{\text{o}} + \frac{[\hat{n} - (\hat{n} \cdot \hat{\beta}_{\text{o}}) \hat{\beta}_{\text{o}}]}{(1 - \hat{n} \cdot \beta_{\text{o}})} \sqrt{1 - \beta_{\text{o}}^2}, \quad (25)$$

where $\hat{\beta}_{\text{o}} \equiv \beta_{\text{o}}/\beta_{\text{o}}$ is the direction of our peculiar velocity (see Section 1). We confirmed numerically that the aberration bias is indeed much smaller than current statistical uncertainties.

⁵The usage of z_{cosmo} in place of z_{cmb} (which is corrected only by our motion with respect to the CMB) also does not entice any statistically significant change.

5. Determination of σ_8 and γ

As discussed in section 3, lensing and PV are essentially uncorrelated. For the JLA catalog, in particular we have divided the sample into three uncorrelated redshift ranges: supernovae lying in the range $z \leq 0.1$ were used in the peculiar velocity analysis; supernovae within $0.1 < z \leq 0.9$ were separated in 8 redshift bins with $\Delta z = 0.1$ and used for the MeMo analysis, and data above $z > 0.9$ were used only to evaluate the background cosmology,⁶ in the standard SALT-2 way. The reason for not using the MeMo for SNe with $z > 0.9$ is twofold. First, there are not many SNe in that range, thus compromising the MeMo method which relies on higher moments. In fact, for $z > 1.0$ there are so few that the sample moments are mathematically ill-defined. For $0.9 < z < 1.0$ we could in principle apply the MeMo, but it was found in [Castro and Quartin \(2014\)](#) that this bin is an outlier in the method, and including it decreases the goodness of fit. Since the origin of this discrepancy is still unknown, we also computed the likelihood including this bin in the MeMo analysis, but results did not change significantly, see [Appendix B](#). The final MeMo likelihood is thus given by:

$$L_{\text{MeMo}} = \prod_{k=1}^8 \frac{1}{(2\pi)^2 \sqrt{|\Sigma_{\text{MeMo}}|}} \exp\left(-\frac{1}{2} \chi_k^2\right), \quad (26)$$

and the total likelihood is

$$L_{\text{tot}} = L_{\text{PV}} L_{\text{MeMo}} L_{z \geq 0.9}. \quad (27)$$

Figure 4 shows the two dimensional contours on $\{\sigma_8, \gamma\}$ for the JLA catalog. In blue are the contours concerning the MeMo analysis. In green we show the PV likelihood plus the background analysis. Finally, in orange is the combination of the two analysis (hereafter, dubbed simply “full analysis”). As can be seen, the PV contours from the real data of the JLA catalog seem to be somewhat in tension with the expectations from CMB assuming GR, to wit $\sigma_8 \simeq 0.8$ and $\gamma = 0.55$. In fact, along the $\gamma = 0.55$ line, we see that PV favors a low σ_8 , in agreement with the recent results of [Huterer et al. \(2015\)](#). Moreover, the PV contours are more vertically oriented than the forecasts with 4000 SNe, leading to only very loose constraints on γ . This

⁶The background analysis is also implicitly contained inside the PV and MeMo methods.

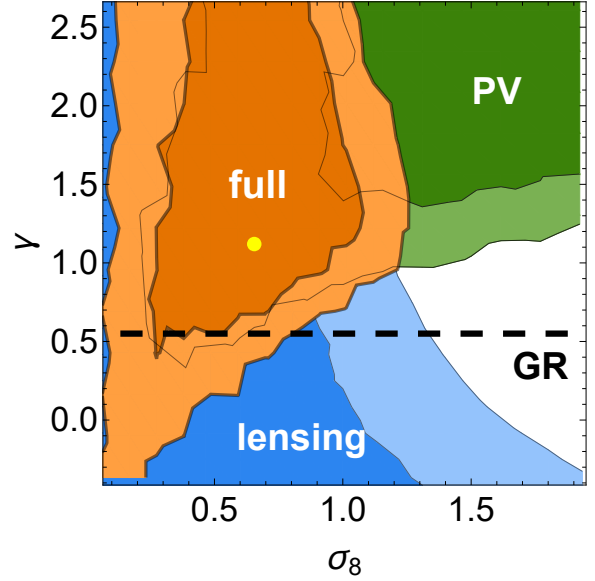


Figure 4: Same as Figure 2 but for the real JLA data. Here, the yellow dot instead represents the best-fit point. Note that the PV contours are in 2σ tension with the expectations from CMB assuming GR, to wit $\sigma_8 \simeq 0.8$ and $\gamma = 0.55$

may suggest that the JLA catalog has some unresolved systematic. We therefore conducted some simple tests, but could not find any hints pointing toward a culprit. We discuss these tests in [Appendix B](#).

It is also important to note that the low statistical significance also means it could be just a random fluctuation. In order to not only test the amplitude of the statistical fluctuations on our combined analysis (and also our code), we conducted tests with mock catalogs. As the PV analysis is computationally intensive, we only investigated 5 such mocks. Each mock had the same spatial distribution of the JLA catalog and very similar statistical properties. More details of these catalogs are presented in [Appendix C](#). Figure 5 shows the two dimensional contours on $\{\sigma_8, \gamma\}$ for these 5 mocks. They seem to be randomly distributed around the fiducial value $\{0.85, 0.55\}$ (presented as a yellow dot) without any clear bias.⁷ Interestingly, one of our 5 mocks (the one with blue contours) show a very similar shape to the real data, again illustrating that the tension in the real data results could be a simple fluke. We also note that the other mocks were able to produce

⁷We also conducted one mock test not including either PV or lensing, and we correctly inferred a value of σ_8 consistent with zero.

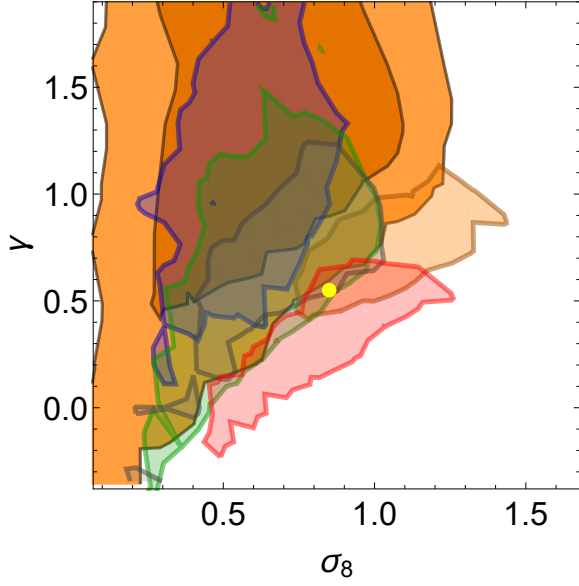


Figure 5: Simulations using mock catalogs of the combined constraints from SNe lensing and PV. In orange we repeat the the 1 and 2σ real data result of Figure 4. The 5 transparent 1σ contours are for 5 different random simulations. The yellow dot marks the fiducial value used in the simulations. Note that one of the 5 mocks produced contours very similar to the real data.

tighter constraints in γ . These large fluctuations in the constraining power should in any case be much smaller with more numerous supernovae catalogs.

Figure 6 illustrates the results of our analysis if we fix the value of either γ or the parameter set $\{\Omega_{b0}, H_0, A, n_s, \tau\}$, the “perturbations” parameters that enter the computation of $P(k)$. Although this is also true for Ω_{c0} , we leave it free in this case otherwise we also fix the background expansion. Both analysis are well motivated: if we suppose that General Relativity is the correct theory of gravitation for cosmology, γ is no longer a free parameter. On the other hand, if we rely on other precise measurements of the perturbation parameters, there is no difference in practice between marginalizing over the priors or fixing them to the best fit. We also show the posterior on the parameter $A \exp(-2\tau)$, from which we derive σ_8 . The contours of $A \exp(-2\tau)$ are depicted in units of the Planck best fit, to wit 1.88×10^{-9} (Ade et al., 2015). This can be directly compared with the recent results of Huterer et al. (2015): the results are similar even though we marginalize over many nuisance parameters.

In figure 7 we show all the one-dimensional con-

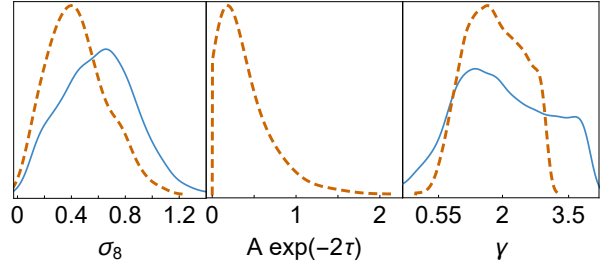


Figure 6: Marginalized 1-dimensional constraints on σ_8 , $A \exp(-2\tau)$ and γ from the combination of SNe lensing and peculiar velocities. In blue we show the full results and in dashed brown the contours obtained by fixing either $\gamma = 0.55$ (i.e. assuming GR) [left and middle] or all perturbation quantities in $P(k)$ [right]. Note that for $\gamma \neq 0.55$ the variable $A \exp(-2\tau)$ is no longer directly related to the amplitude at the LSS, so we only plot the GR case contours for it.

straints on the other twelve parameters. This figure exhibits the robustness of our results, illustrating that our chain covered all the high-likelihood region. More details of our MCMC analysis are provided in Appendix A. In Table 1 we summarize our main results: the measurements of σ_8 and γ . For the full analysis our best fit for σ_8 is in agreement with the values obtained with the CMB. However, traditional CMB analysis concerns the case of fixed γ , and in that case our best-fit is in roughly 2σ tension with the values obtained by Planck (Ade et al., 2015). We come back to this issue below when we compare the full contours of SNe and other datasets.

The values of γ in Table 1 for the full analysis are consistent with GR but the precision achieved is still worse compared to other results in literature: Mantz et al. (2015) found $\gamma = 0.48 \pm 0.19$ using only X-ray clusters number counts; Bocquet et al. (2015) on the other hand obtained $\gamma = 0.73 \pm 0.28$ from a cluster sample selected in SPT survey through the Sunyaev Zel’dovich effect. Abate and Lahav (2008) also used SNe PV to constrain γ but did so fixing all other variables. They obtained $\gamma = 0.72 \pm 0.21$, a result with much higher precision than ours in the case of fixed perturbation parameters, where although our constraints on γ are tighter they are still over twice as large as their result (and in 2.3σ tension with GR). Finally, we note that JLA SNe have been used before to put constraints on γ by Amendola et al. (2015) resulting in $\gamma = 0.52^{+0.16}_{-0.13}$, although in that paper this was driven mostly by the inclusion of redshift-space distortions from a collection of galaxy surveys.

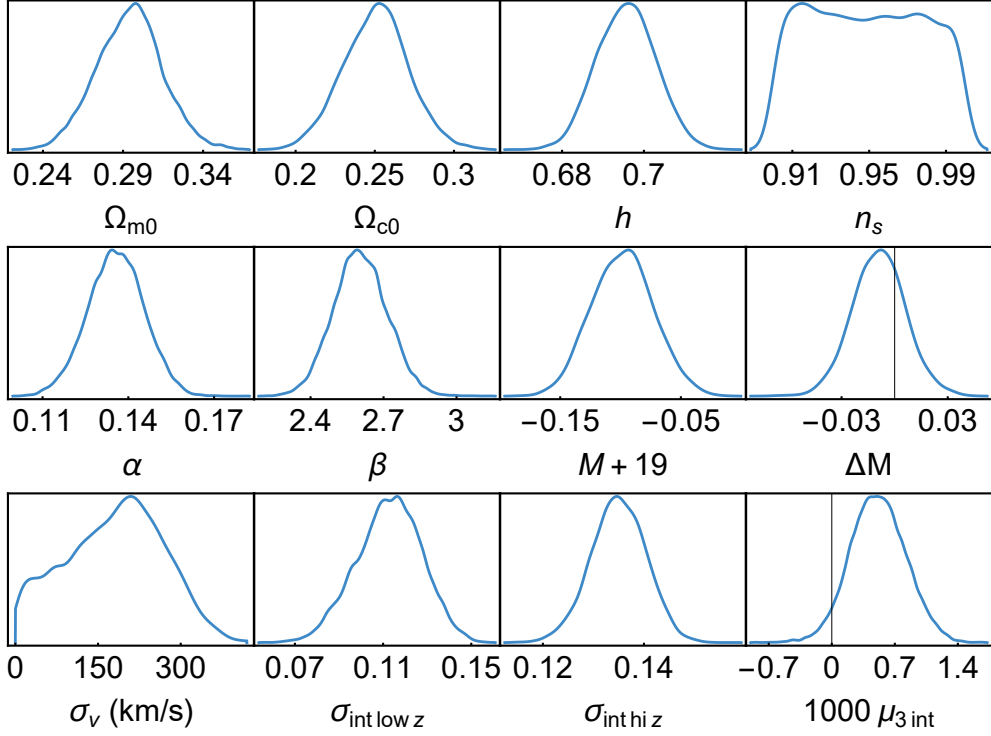


Figure 7: Marginalized 1-dimensional constraints from the combination of SNe lensing and peculiar velocities (PV). We only adopted tight priors for h and Ω_{b0} . For n_s we used a top-hat in the region $[0.9, 1.0]$. All other variables had broad flat priors. The σ_{int} parameters are in mag, and $\mu_{3,\text{int}}$ in mag^3 .

	Full	Fixed pert. vars.	Fixed γ
σ_8	$0.65^{+0.23}_{-0.34}$	0.79 ± 0.07 (prior)	$0.40^{+0.21}_{-0.23}$
γ	$1.38^{+1.7}_{-0.65}$	$1.62^{+0.89}_{-0.55}$	0.55 (prior)

Table 1: Marginalized measurements of σ_8 and γ from the combination of SNe lensing and peculiar velocities (PV). The first column is the general result; the second and third columns represent the cases in which we fixed the either γ or all the perturbation variables in $P(k)$ to their fiducial values, together with the corresponding priors.

We depict in Figure 8 a direct comparison of the SNe constraints with constraints from 3 other datasets, as obtained in Mantz et al. (2015). The three external datasets consist of Planck CMB power spectra (complemented by large-scale WMAP polarization), X-ray selected cluster masses and galaxy surveys (both redshift-space distortions and Alcock–Paczynski effects). We refer the reader to Mantz et al. (2015) for more details. In order to construct this plot, we reverse engineered the contours from Fig. B1 of their paper, interpolating the overlapped regions. Although current SNe data do

not provide competitive constraints, it is interesting to see that even in the near future⁸ the statistical power on SNe will be very competitive and complement well for instance the Planck CMB contours, which in fact only achieve the quoted percent-level measurements of σ_8 (Ade et al., 2015) by assuming $\gamma \equiv 0.55$.

We find the results here presented to be specially interesting because they show that SNe data alone will be capable in the near-future of constraining σ_8 and γ , in addition to the standard background quantities. Moreover, the results obtained with current data may indicate that a systematic is still unresolved, and our analysis is exercising a nice cross-check role. It is worth noting that we carried here a conservative analysis, in the sense that our results were marginalized over all nuisance parameters which are often left fixed in literature.

⁸DES is already commissioning and a couple of low- z SN project releases are expected for the next years, such as Supernovae Factory (Aldering et al., 2006), Carnegie Supernovae Project (Hamuy et al., 2006), La Silla/QUEST (Hadjijyska et al., 2012), SkyMapper (Keller et al., 2007), and Palomar Transient Factory (Law et al., 2009).

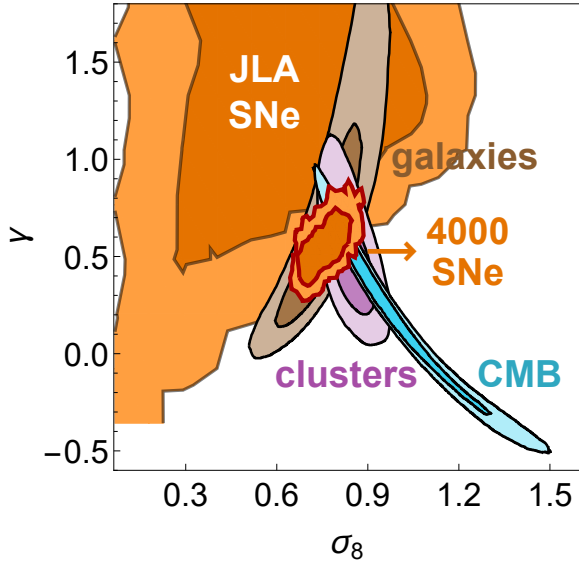


Figure 8: Comparison of the constraints on σ_8 and γ from supernovae (using lensing and PV), Planck CMB spectra, clusters and galaxies. The large orange contours are for the JLA supernovae, whereas the smaller orange contours with red borders are a forecast for DES + 1000 low- z SNe, as discussed in Section 3. The non-SNe contours were obtained by Mantz et al. (2015). Note that current SNe are already able to complement well the other data, specially the CMB.

6. Conclusions

In this paper we present current constraints and future forecasts on the matter power spectrum and growth of structure using supernovae data only. To do so, we split the JLA supernovae catalog in three redshift ranges. Nearby supernovae ($z < 0.1$) were analyzed evaluating their peculiar velocity correlations (described in Section 2). Supernovae farther away ($0.1 < z < 0.9$) were analyzed extracting their weak-lensing induced non-Gaussianity distribution (see Section 1). Finally, for the few supernovae with $z > 0.9$ (which apparently are not well modeled by our lensing method), the standard background analysis was adopted. In our analysis we marginalized over all parameters of ignorance, including the light-curve fitting ones. We thus take them to be very robust.

The peculiar velocity and lensing analysis are both sensitive to the power spectrum and its evolution, but on their own both have pronounced degeneracies between not only these parameters but also with the background ones. On the other hand, the standard SN analysis are completely insensitive to any perturbation parameters and just constrain

the background cosmology. We showed that in the near-future by combining these three probes not only all these degeneracies will be broken, as can be seen in Figure 2, but also competitive constraints will be achieved due to an almost orthogonal degeneracy between lensing and PV contours.

Our results for the JLA catalog were not as expected. The PV analysis produced results in roughly 2σ tension with expectations from CMB assuming GR. On the other hand, similar results were also obtained with 1 of our 5 mock catalogs. A robust assessment of this tension would require running at the very least dozens of such mock analysis, but this is a computationally intensive task and we did not have the resources to execute. In any case, we also see that some of the other JLA mocks produced much tighter constraints in γ , so if the current tension is not due to unknown systematics, future SN catalogs have the ability to put much tighter constraints in γ .

In closing, the combination of PV and lensing opens a new possibility of analysis capable of constraining both the present matter power spectrum and its growth using only supernova data. This combined method has a great potential in the future as the largest current catalog still constitutes but a small fraction of the total number of SN explosions that occur every year.

Note Added

In the analysis in the original pre-print version of this manuscript we had a bug in our code [a simple sign error in β_0 in eq. (2)] that coincidentally shifted our results to be more in agreement with expectations from GR and CMB (and also with one of our mock catalogs). Since β_0 was not included in our mocks, their results were not affected by this bug and we thus missed it.

Acknowledgments

We would like to thank Alex Conley for providing helpful insights and clarifications on the JLA data and Dragan Huterer, Daniel Shafera and Fabian Schmidt for pointing out imprecisions in the original version of this manuscript: this motivated us to search and find a bug in our code. It is also a pleasure to acknowledge Beatriz Siffert, Maurício Calvão and Ribamar Reis for fruitful discussions. TC is supported by the Brazilian research agency

CAPES. MQ is supported by Brazilian research agencies CNPq and FAPERJ. SB is supported by Brazilian research agency CNPq.

References

- Abate, A., Lahav, O., 2008. The Three Faces of Ω_m : Testing Gravity with Low and High Redshift SN Ia Surveys. *Mon. Not. Roy. Astron. Soc.* 389, 47. doi:[10.1111/j.1745-3933.2008.00519.x](#), [arXiv:0805.3160](#).
- Abell, P.A., et al. (LSST Science Collaborations, LSST Project), 2009. LSST Science Book, Version 2.0 [arXiv:0912.0201](#).
- Adam, R., et al. (Planck), 2015. Planck 2015 results. VIII. High Frequency Instrument data processing: Calibration and maps [arXiv:1502.01587](#).
- Ade, P.A.R., et al. (Planck), 2015. Planck 2015 results. XIII. Cosmological parameters [arXiv:1502.01589](#).
- Aghanim, N., et al. (Planck), 2014. Planck 2013 results. XXVII. Doppler boosting of the CMB: Eppure si muove. *Astron.Astrophys.* 571, A27. doi:[10.1051/0004-6361/201321556](#), [arXiv:1303.5087](#).
- Aldering, G., et al. (Nearby Supernova Factory), 2006. Nearby Supernova Factory Observations of SN 2005gj: Another Type Ia Supernova in a Massive Circumstellar Envelope. *Astrophys. J.* 650, 510–527. doi:[10.1086/507020](#), [arXiv:astro-ph/0606499](#).
- Amendola, L., Castro, T., Marra, V., Quartin, M., 2015. Constraining the growth of perturbations with lensing of supernovae. *Mon. Not. Roy. Astron. Soc.* 449, 2845–2852. doi:[10.1093/mnras/stv497](#), [arXiv:1412.3703](#).
- Amendola, L., Catena, R., Masina, I., Notari, A., Quartin, M., Quercellini, C., 2011. Measuring our peculiar velocity on the CMB with high-multipole off-diagonal correlations. *JCAP* 1107, 027. doi:[10.1088/1475-7516/2011/07/027](#), [arXiv:1008.1183](#).
- Amendola, L., Kainulainen, K., Marra, V., Quartin, M., 2010. Large-scale inhomogeneities may improve the cosmic concordance of supernovae. *Phys.Rev.Lett.* 105, 121302. doi:[10.1103/PhysRevLett.105.121302](#), [arXiv:1002.1232](#).
- Amendola, L., Tsujikawa, S., 2010. *Dark Energy: Theory and Observations*. Cambridge University Press.
- Bahcall, N.A., Ostriker, J.P., Perlmutter, S., Steinhardt, P.J., 1999. The Cosmic triangle: Assessing the state of the universe. *Science* 284, 1481–1488. doi:[10.1126/science.284.5419.1481](#), [arXiv:astro-ph/9906463](#).
- Ben-Dayan, I., Gasperini, M., Marozzi, G., Nugier, F., Veneziano, G., 2013. Average and dispersion of the luminosity-redshift relation in the concordance model. *JCAP* 1306, 002. doi:[10.1088/1475-7516/2013/06/002](#), [arXiv:1302.0740](#).
- Bennett, C.L., Larson, D., Weiland, J.L., Hinshaw, G., 2014. The 1% Concordance Hubble Constant. *Astrophys. J.* 794, 135. doi:[10.1088/0004-637X/794/2/135](#), [arXiv:1406.1718](#).
- Bernardeau, F., Van Waerbeke, L., Mellier, Y., 1997. Weak lensing statistics as a probe of Omega and power spectrum. *Astron.Astrophys.* 322, 1–18. [arXiv:astro-ph/9609122](#).
- Bernstein, J., Kessler, R., Kuhlmann, S., Biswas, R., Kovacs, E., et al., 2012. Supernova Simulations and Strategies for the Dark Energy Survey. *Astrophys.J.* 753, 152. doi:[10.1088/0004-637X/753/2/152](#), [arXiv:1111.1969](#).
- Betoule, M., et al. (SDSS Collaboration), 2014. Improved cosmological constraints from a joint analysis of the SDSS-II and SNLS supernova samples. *Astron.Astrophys.* 568, A22. doi:[10.1051/0004-6361/201423413](#), [arXiv:1401.4064](#).
- Blake, C., et al., 2011. The WiggleZ Dark Energy Survey: mapping the distance-redshift relation with baryon acoustic oscillations. *MNRAS* 418, 1707–1724. doi:[10.1111/j.1365-2966.2011.19592.x](#), [arXiv:1108.2635](#).
- Bocquet, S., et al. (SPT), 2015. Mass Calibration and Cosmological Analysis of the SPT-SZ Galaxy Cluster Sample Using Velocity Dispersion σ_v and X-ray Y_X Measurements. *Astrophys. J.* 799, 214. doi:[10.1088/0004-637X/799/2/214](#), [arXiv:1407.2942](#).
- Bolejko, K., Clarkson, C., Maartens, R., Bacon, D., Meures, N., Beynon, E., 2013. Antilensing: The Bright Side of Voids. *Phys. Rev. Lett.* 110, 021302. doi:[10.1103/PhysRevLett.110.021302](#), [arXiv:1209.3142](#).
- Bonvin, C., Durrer, R., Gasparini, M.A., 2006. Fluctuations of the luminosity distance. *Phys. Rev. D* 73, 023523. doi:[10.1103/PhysRevD.73.023523](#), [arXiv:astro-ph/0511183](#). [Erratum: *Phys. Rev.D* 85, 029901(2012)].
- Castro, T., Quartin, M., 2014. First measurement of σ_8 using supernova magnitudes only. *MNRAS* 443, L6–L10. doi:[10.1093/mnras/ltu071](#), [arXiv:1403.0293](#).
- Challinor, A., van Leeuwen, F., 2002. Peculiar velocity effects in high resolution microwave background experiments. *Phys.Rev. D* 65, 103001. doi:[10.1103/PhysRevD.65.103001](#), [arXiv:astro-ph/0112457](#).
- Conley, A., et al., 2011. Supernova Constraints and Systematic Uncertainties from the First Three Years of the Supernova Legacy Survey. *ApJS* 192, 1. doi:[10.1088/0067-0049/192/1/1](#), [arXiv:1104.1443](#).
- Courtin, J., Rasera, Y., Alimi, J.M., Corasaniti, P.S., Boucher, V., et al., 2011. Imprints of dark energy on cosmic structure formation: II) Non-Universality of the halo mass function. *Mon.Not.Roy.Astron.Soc.* 410, 1911–1931. doi:[10.1111/j.1365-2966.2010.17573.x](#), [arXiv:1001.3425](#).
- Davis, T.M., et al., 2011. The Effect of Peculiar Velocities on Supernova Cosmology. *ApJ* 741, 67. doi:[10.1088/0004-637X/741/1/67](#), [arXiv:1012.2912](#).
- Dodelson, S., Vallinotto, A., 2006. Learning from the scatter in type ia supernovae. *Phys.Rev. D* 74, 063515. doi:[10.1103/PhysRevD.74.063515](#), [arXiv:astro-ph/0511086](#).
- Eisenstein, D.J., et al., 2005. Detection of the Baryon Acoustic Peak in the Large-Scale Correlation Function of SDSS Luminous Red Galaxies. *ApJ* 633, 560–574. doi:[10.1086/466512](#), [arXiv:arXiv:astro-ph/0501171](#).
- Gordon, C., Land, K., Slosar, A., 2007. Cosmological Constraints from Type Ia Supernovae Peculiar Velocity Measurements. *Physical Review Letters* 99, 081301. doi:[10.1103/PhysRevLett.99.081301](#), [arXiv:0705.1718](#).
- Guy, J., Astier, P., Baumont, S., Hardin, D., Pain, R., et al., 2007. SALT2: Using distant supernovae to improve the use of Type Ia supernovae as distance indicators. *Astron.Astrophys.* 466, 11–21. doi:[10.1051/0004-6361:20066930](#), [arXiv:astro-ph/0701828](#).
- Hadjiyska, E., Rabinowitz, D., Baltay, C., Ellman, N., Nugent, P., Zinn, R., Horowitz, B., McKinnon, R., Miller, L.R., 2012. La Silla-QUEST Variability Survey in the Southern Hemisphere, in: Griffin, E., Hanisch, R., Sea-

- man, R. (Eds.), *New Horizons in Time Domain Astronomy*, pp. 324–326. doi:[10.1017/S1743921312000944](https://doi.org/10.1017/S1743921312000944), [arXiv:1210.1584](https://arxiv.org/abs/1210.1584).
- Hamana, T., Futamase, T., 2000. A new measure of σ_8 using the lensing dispersion in high- z type Ia sne. *ApJ* 534, 29–33. doi:[10.1086/308758](https://doi.org/10.1086/308758), [arXiv:astro-ph/9912319](https://arxiv.org/abs/astro-ph/9912319).
- Hamuy, M., Phillips, M.M., Suntzeff, N.B., Schommer, R.A., Maza, J., Aviles, R., 1996. The absolute luminosities of the calan/tololo type Ia supernovae. *AJ* 112, 2391–2397. doi:[10.1086/118190](https://doi.org/10.1086/118190), [arXiv:astro-ph/9609059](https://arxiv.org/abs/astro-ph/9609059).
- Hamuy, M., et al., 2006. The carnegie supernova project: the low-redshift survey. *Publ. Astron. Soc. Pac.* 118, 2–20. doi:[10.1086/500228](https://doi.org/10.1086/500228), [arXiv:astro-ph/0512039](https://arxiv.org/abs/astro-ph/0512039).
- Hannestad, S., Haugboelle, T., Thomsen, B., 2008. Precision measurements of large scale structure with future type Ia supernova surveys. *JCAP* 0802, 022. doi:[10.1088/1475-7516/2008/02/022](https://doi.org/10.1088/1475-7516/2008/02/022), [arXiv:0705.0979](https://arxiv.org/abs/0705.0979).
- Hilbert, S., White, S.D., Hartlap, J., Schneider, P., 2008. Strong lensing optical depths in a LCDM Universe. 2. The influence of the stellar mass in galaxies. *Mon. Not. Roy. Astron. Soc.* 386, 1845–1854. doi:[10.1111/j.1365-2966.2008.13190.x](https://doi.org/10.1111/j.1365-2966.2008.13190.x), [arXiv:0712.1593](https://arxiv.org/abs/0712.1593).
- Hoffman, Y., Courtois, H.M., Tully, R.B., 2015. Cosmic Bulk Flow and the Local Motion from Cosmicflows-2. *Mon. Not. Roy. Astron. Soc.* 449, 4494–4505. doi:[10.1093/mnras/stv615](https://doi.org/10.1093/mnras/stv615), [arXiv:1503.05422](https://arxiv.org/abs/1503.05422).
- Holz, D.E., Linder, E.V., 2005. Safety in numbers: Gravitational lensing degradation of the luminosity distance-redshift relation. *Astrophys. J.* 631, 678–688. doi:[10.1086/432085](https://doi.org/10.1086/432085), [arXiv:astro-ph/0412173](https://arxiv.org/abs/astro-ph/0412173).
- Hudson, M.J., Smith, R.J., Lucey, J.R., Branchini, E., 2004. Streaming motions of galaxy clusters within 12000 km s⁻¹. 5. The Peculiar velocity field. *Mon. Not. Roy. Astron. Soc.* 352, 61. doi:[10.1111/j.1365-2966.2004.07893.x](https://doi.org/10.1111/j.1365-2966.2004.07893.x), [arXiv:astro-ph/0404386](https://arxiv.org/abs/astro-ph/0404386).
- Hui, L., Greene, P.B., 2006. Correlated fluctuations in luminosity distance and the importance of peculiar motion in supernova surveys. *PRD* 73, 123526. doi:[10.1103/PhysRevD.73.123526](https://doi.org/10.1103/PhysRevD.73.123526), [arXiv:astro-ph/0512159](https://arxiv.org/abs/astro-ph/0512159).
- Huterer, D., Shafer, D.L., Schmidt, F., 2015. No evidence for bulk velocity from type Ia supernovae [arXiv:1509.04708](https://arxiv.org/abs/1509.04708).
- Iocco, F., Mangano, G., Miele, G., Pisanti, O., Serpico, P.D., 2009. Primordial Nucleosynthesis: from precision cosmology to fundamental physics. *Phys. Rept.* 472, 1–76. doi:[10.1016/j.physrep.2009.02.002](https://doi.org/10.1016/j.physrep.2009.02.002), [arXiv:0809.0631](https://arxiv.org/abs/0809.0631).
- Jenkins, A., Frenk, C., White, S.D., Colberg, J., Cole, S., et al., 2001. The Mass function of dark matter halos. *Mon. Not. Roy. Astron. Soc.* 321, 372. doi:[10.1046/j.1365-8711.2001.04029.x](https://doi.org/10.1046/j.1365-8711.2001.04029.x), [arXiv:astro-ph/0005260](https://arxiv.org/abs/astro-ph/0005260).
- Jönsson, J., Dahlén, T., Hook, I., Goobar, A., Mörtzell, E., 2010a. Weighing dark matter haloes with gravitationally lensed supernovae. *Mon. Not. Roy. Astron. Soc.* 402, 526–536. doi:[10.1111/j.1365-2966.2009.15907.x](https://doi.org/10.1111/j.1365-2966.2009.15907.x), [arXiv:0910.4098](https://arxiv.org/abs/0910.4098).
- Jönsson, J., Sullivan, M., Hook, I., Basa, S., Carlberg, R., et al., 2010b. Constraining dark matter halo properties using lensed SNLS supernovae. *Mon. Not. Roy. Astron. Soc.* 405, 535–544. doi:[10.1111/j.1365-2966.2010.16467.x](https://doi.org/10.1111/j.1365-2966.2010.16467.x), [arXiv:1002.1374](https://arxiv.org/abs/1002.1374).
- Kainulainen, K., Marra, V., 2009. A new stochastic approach to cumulative weak lensing. *Phys. Rev. D* 80, 123020. doi:[10.1103/PhysRevD.80.123020](https://doi.org/10.1103/PhysRevD.80.123020), [arXiv:0909.0822](https://arxiv.org/abs/0909.0822).
- Kainulainen, K., Marra, V., 2011. Accurate Modeling of Weak Lensing with the sGL Method. *Phys. Rev. D* 83, 023009. doi:[10.1103/PhysRevD.83.023009](https://doi.org/10.1103/PhysRevD.83.023009), [arXiv:1011.0732](https://arxiv.org/abs/1011.0732).
- Keller, S.C., et al., 2007. SkyMapper and the Southern Sky Survey. *Publ. Astron. Soc. Austral.* 24, 1–12. doi:[10.1071/AS07001](https://doi.org/10.1071/AS07001), [arXiv:astro-ph/0702511](https://arxiv.org/abs/astro-ph/0702511).
- Kosowsky, A., Kahnashvili, T., 2011. The Signature of Proper Motion in the Microwave Sky. *Phys. Rev. Lett.* 106, 191301. doi:[10.1103/PhysRevLett.106.191301](https://doi.org/10.1103/PhysRevLett.106.191301), [arXiv:1007.4539](https://arxiv.org/abs/1007.4539).
- Lahav, O., Lilje, P.B., Primack, J.R., Rees, M.J., 1991. Dynamical effects of the cosmological constant. *MNRAS* 251, 128–136.
- Law, N.M., et al., 2009. The Palomar Transient Factory: System Overview, Performance and First Results. *Publ. Astron. Soc. Pac.* 121, 1395. doi:[10.1086/648598](https://doi.org/10.1086/648598), [arXiv:0906.5350](https://arxiv.org/abs/0906.5350).
- Lewis, A., Challinor, A., Lasenby, A., 2000. Efficient Computation of CMB anisotropies in closed FRW models. *Astrophys. J.* 538, 473–476. doi:[10.1086/309179](https://doi.org/10.1086/309179), [arXiv:astro-ph/9911177](https://arxiv.org/abs/astro-ph/9911177).
- Mantz, A.B., et al., 2015. Weighing the giants – IV. Cosmology and neutrino mass. *Mon. Not. Roy. Astron. Soc.* 446, 2205–2225. doi:[10.1093/mnras/stu2096](https://doi.org/10.1093/mnras/stu2096), [arXiv:1407.4516](https://arxiv.org/abs/1407.4516).
- Marra, V., Quartin, M., Amendola, L., 2013. Accurate weak lensing of standard candles. I. Flexible cosmological fits. *Phys. Rev. D* 88, 063004. doi:[10.1103/PhysRevD.88.063004](https://doi.org/10.1103/PhysRevD.88.063004), [arXiv:1304.7689](https://arxiv.org/abs/1304.7689).
- Neill, J.D., Hudson, M.J., Conley, A.J. (SNLS), 2007. The Peculiar Velocities of Local Type Ia Supernovae and their Impact on Cosmology. *Astrophys. J.* 661, L123. doi:[10.1086/518808](https://doi.org/10.1086/518808), [arXiv:0704.1654](https://arxiv.org/abs/0704.1654).
- Notari, A., Quartin, M., 2012. Measuring our Peculiar Velocity by ‘Pre-deboosting’ the CMB. *JCAP* 1202, 026. doi:[10.1088/1475-7516/2012/02/026](https://doi.org/10.1088/1475-7516/2012/02/026), [arXiv:1112.1400](https://arxiv.org/abs/1112.1400).
- Perlmutter, S., others, The Supernova Cosmology Project, 1999. Measurements of Omega and Lambda from 42 high-redshift supernovae. *ApJ* 517, 565–586. doi:[10.1086/307221](https://doi.org/10.1086/307221), [arXiv:astro-ph/9812133](https://arxiv.org/abs/astro-ph/9812133).
- Quartin, M., Marra, V., Amendola, L., 2014. Accurate Weak Lensing of Standard Candles. II. Measuring σ_8 with Supernovae. *Phys. Rev. D* 89, 023009. doi:[10.1103/PhysRevD.89.023009](https://doi.org/10.1103/PhysRevD.89.023009), [arXiv:1307.1155](https://arxiv.org/abs/1307.1155).
- Riess, A.G., Press, W.H., Kirshner, R.P., 1996. A precise distance indicator: Type Ia supernova multicolor light-curve shapes. *ApJ* 473, 88–109. doi:[10.1086/178129](https://doi.org/10.1086/178129), [arXiv:astro-ph/9604143](https://arxiv.org/abs/astro-ph/9604143).
- Riess, A.G., et al., 1998. Observational evidence from supernovae for an accelerating universe and a cosmological constant. *AJ* 116, 1009–1038. doi:[10.1086/300499](https://doi.org/10.1086/300499), [arXiv:astro-ph/9805201](https://arxiv.org/abs/astro-ph/9805201).
- Sheth, R.K., Tormen, G., 1999. Large scale bias and the peak background split. *Mon. Not. Roy. Astron. Soc.* 308, 119. doi:[10.1046/j.1365-8711.1999.02692.x](https://doi.org/10.1046/j.1365-8711.1999.02692.x), [arXiv:astro-ph/9901122](https://arxiv.org/abs/astro-ph/9901122).
- Takahashi, R., Oguri, M., Sato, M., Hamana, T., 2011. Probability Distribution Functions of Cosmological Lensing: Convergence, Shear, and Magnification. *Astrophys. J.* 742, 15. doi:[10.1088/0004-637X/742/1/15](https://doi.org/10.1088/0004-637X/742/1/15), [arXiv:1106.3823](https://arxiv.org/abs/1106.3823).
- Valageas, P., 2000. Statistical properties of the convergence due to weak gravitational lensing by nonlinear structures. *Astron. Astrophys.* 356, 771. [arXiv:astro-ph/9911336](https://arxiv.org/abs/astro-ph/9911336).
- Yoon, M., Huterer, D., 2015. Kinematic dipole detection with galaxy surveys: forecasts and requirements. *Astrophys. J.* 813, L18. doi:[10.1088/2041-8205/813/1/L18](https://doi.org/10.1088/2041-8205/813/1/L18), [arXiv:1509.05374](https://arxiv.org/abs/1509.05374).

Zhao, D., Jing, Y., Mo, H., Boerner, G., 2009. Accurate universal models for the mass accretion histories and concentrations of dark matter halos. *Astrophys.J.* 707, 354–369. doi:[10.1088/0004-637X/707/1/354](https://doi.org/10.1088/0004-637X/707/1/354), [arXiv:0811.0828](https://arxiv.org/abs/0811.0828).

Appendix A. MCMC details

In this paper we used a Markov Chain Monte Carlo (MCMC) method to obtain samples from the posterior distribution of the parameters. Our MCMC code consists in a flexible implementation of the Metropolis–Hastings algorithm. It has been previously tested with many different likelihood functions, confronting the results with a simpler, grid-based likelihood code.

The chains used in this work were systematically produced following a careful algorithm. For any chain we always run a previous chain, where we discarded the first half of the points (the MCMC “burn-in” stage) and computed the covariance from the last points. Subsequently, we run a new chain from where we had previously stopped using the covariance of the previous chain as the covariance of our trial function. In that way our final chain was not only burn-in free but also more efficient due to the more accurate trial function.

All the chains are available for download.⁹

Appendix B. Search for systematics

We tested the possibility of a few unresolved systematics being present in the JLA catalog, and whether the supernovae PV analysis demands extra parameters in order to produce better fits (or in better agreement with our mock results).

Regarding possible unresolved systematics we realize that low- z supernovae comes from both SDSS sub-sample as well as the so-called low- z sample. The latter is a compilation of several SNe observed from different surveys with different technical specification. Suspecting that this compilation could add some spurious correlation we analyzed both SDSS and low- z SNe separately. However, the results did not present any noticeable difference.

Regarding the need for extra nuisance variables in the SN PV analysis, we tested adding a new variable λ that parametrizes the non-linear peculiar velocities as $\sigma_{PV}(z) = \sigma_{PV,0} + \lambda z$. This could be physically motivated as non-linear velocities of

deeper supernovae should be smaller since deviations of $P(k)$ from the linear approximation also becomes smaller; again, our results did not present any noticeable change in the cosmological parameters, and the constraints on λ were fully consistent with 0.

Finally, as discussed in Section 5, we also investigated whether adding back the bin with $z \in [0.9, 1.0]$ changed the results significantly. We found that it did not. The most significant change was a slight shift upwards for σ_8 . After marginalizing over all other parameters (including γ) we got $\sigma_8 = 0.79 \pm 0.28$.

Appendix C. Mock Catalogs

To generate the mock catalogs, we first assumed a magnitude distribution given by a fiducial Λ CDM model in GR (i.e., $\gamma = 0.55$) with $\{\sigma_8 = 0.85, \Omega_{m0} = 0.289, h = 0.7\}$. Then for all SNe with $z \leq 0.1$ we added the PV effects, employing the code made available in [Hui and Greene \(2006\)](#) to compute the covariance. We added to the diagonal of the covariance an intrinsic dispersion of $\sigma_{\text{int}} = 0.13$ mag and used the inverse of the resulting covariance to draw random realizations of a multi-normal Gaussian. For all SNe with $0.1 < z \leq 0.9$ we added instead uncorrelated random dispersions given by the MeMo covariance matrix of (17), also computed assuming $\sigma_{\text{int}} = 0.13$ mag (and $\mu_{N,\text{int}} = 0$ for all $N > 2$).

Although the lensing PDF is sometimes approximated by a log-normal distribution, this is not a good enough approximation to accurately compute the MeMo lensing covariance when using the first 4 moments of the distribution. In particular [Marra et al. \(2013\)](#) provided fits for both the central moments of the lensing PDF and for the approximate log-normal distribution. The latter, however, does not provide accurate prescriptions for the higher moments. It introduces biases in the analysis and it is unsuitable for generating good mock catalogs. For mocks, one instead has to rely on the full results for the first 8 moments computed with [turboGL](#) (see Section 3). We thus turned to the results originally obtained in [Amendola et al. \(2015\)](#), where [turboGL](#) was used to compute the lensing moments as a function of $\{z, \Omega_{m0}, \sigma_8, \gamma\}$.

Finally, we combined the lensing simulations described above with the PV covariance using the code created by [Hui and Greene \(2006\)](#), as described in Section 3.

⁹<http://sites.if.ufrj.br/castro/en/pesquisa/artigos/>